

Evaluation of a Scalar Eddy Transport Coefficient Based on Geometric Constraints

S.D. Bachman^a, D.P. Marshall^b, J.R. Maddison^c, J. Mak^c

^a*Department of Applied Mathematics and Theoretical Physics, University of Cambridge, UK*

^b*Department of Physics, University of Oxford, UK*

^c*School of Mathematics and Maxwell Institute for Mathematical Sciences, University of Edinburgh, UK*

Abstract

A suite of idealized models is used to evaluate and compare several previously proposed scalings for the eddy transport coefficient in downgradient mesoscale eddy closures. Of special interest in this comparison is a scaling introduced as part of the eddy parameterization framework of Marshall et al. (2012), which is derived using the inherent geometry of the Eliassen–Palm eddy flux tensor. The primary advantage of using this coefficient in a downgradient closure is that all dimensional terms are explicitly specified and the only uncertainty is a nondimensional parameter, α , which is bounded by one in magnitude.

In each model a set of passive tracers is initialized, whose flux statistics are used to invert for the eddy-induced tracer transport. Unlike previous work, where this technique has been employed to diagnose the tensor coefficient of a linear flux-gradient relationship, the idealization of these models allows the lateral eddy transport to be described by a scalar coefficient. The skill of the extant scalings is then measured by comparing their predicted values against the coefficients diagnosed using this method. The Marshall et al. (2012) scaling is shown to scale most closely with the diagnosed coefficients across all simulations. It is shown that the skill of this scaling is due to its functional dependence on the total eddy energy, and that this scaling provides an excellent match to the diagnosed fluxes even in the limit of constant α . Possible extensions to this work, including how to incorporate the resultant transport coefficient into the Gent and McWilliams parameterization, are discussed.

Keywords: quasigeostrophic; residual mean; eddy; parameterization; Gent and McWilliams; diffusivity

1. Introduction

The development of ocean eddy parameterizations continues to be an area of vigorous research. The ubiquity of geostrophic ocean eddies, and the central role they play in shaping the mean circulation, stratification, and transport of tracers of the ocean (e.g. Danabasoglu et al., 1994; Henning and Vallis, 2004; Marshall and Speer, 2012; Lauderdale et al., 2013), implies that the skill of eddy parameterizations can have a significant effect on the accuracy of future climate predictions. Furthermore, it is likely that parameterizations will be necessary even for the largest-scale ocean eddies well into the foreseeable future. To resolve the geostrophic eddy field and accurately represent the complex interactions between these eddies and the

*Corresponding Author address: Scott Bachman, DAMTP, Centre for Mathematical Sciences, Wilberforce Road, Cambridge CB3 0WA, United Kingdom; E-mail: sb965@cam.ac.uk; Phone: +44 01223 765997

large-scale circulation requires model grid spacings at least an order of magnitude finer than the dominant energy-containing scales. Even in the mid-latitudes, where the dominant eddy scale is approximately 100 km (Stammer, 1997; Chelton et al., 1998), for a model to be considered “mesoscale eddy-resolving” requires a grid spacing of less than 10 km (Hecht and Smith, 2008; Hallberg, 2013), beyond the capability of current climate-scale ocean models.

A longstanding approach to the eddy parameterization problem is to consider the resolved flow as an averaged or filtered representation of the true flow field. For a Cartesian-coordinate model, after applying the standard Reynolds averaging axioms to the primitive equations the resulting equation set contains an eddy flux divergence in each of the constituent equations, each of which must be parameterized. It has heretofore been common to develop parameterizations for each eddy flux individually, rather than developing a single, unified parameterization for the full set of eddy fluxes. The downside of this approach is that a model may feature several potentially inconsistent eddy parameterizations, where answers to practical questions such as how these parameterizations interact are often unknown.

Because of these difficulties, it is advantageous to try to reduce the number of required parameterizations by grouping the eddy forcing into as few equations as possible. The residual-mean formalism (e.g. Andrews and McIntyre, 1976; Andrews, 1983; de Szoeke and Bennett, 1993; McDougall and McIntosh, 2001; Young, 2012; Maddison and Marshall, 2013) is one means by which this can be achieved through careful averaging and the appropriate definition of a residual circulation. In addition to their mathematical elegance, the residual-mean equations have shown promise as a platform for ocean model development in scenarios where knowledge of the Eulerian velocity is not necessary (e.g. Wardle and Marshall, 2000; Ferreira and Marshall, 2006; Zhao and Vallis, 2008).

With regard to the eddy parameterization problem, it has been shown by Marshall et al. (2012) that the quasigeostrophic (QG) residual-mean formalism can be used to develop a framework for eddy parameterization which conserves momentum and satisfies important energy constraints. A subtle yet important feature of this framework is that the problem of understanding, quantifying, and parameterizing eddy-mean flow interaction can be effectively recast as a problem of understanding the underlying geometry of the eddy fluxes themselves. The Eliassen–Palm flux tensor (hereafter “EP tensor”), which is introduced in Section 2.1 and described in detail in Maddison and Marshall (2013), is a fundamental object describing this geometry, and among its noteworthy features is that it can be chosen such that the resultant eddy stresses are nonzero only in the horizontal momentum equations. From a practical point of view this offers significant advantages for the development of eddy parameterizations, allowing a modeler to avoid imposing separate (and possibly physically inconsistent) parameterizations in the momentum and buoyancy equations.

As of the writing of this paper, no single eddy closure has been developed which skillfully parameterizes each of the terms in the EP tensor in a unified and consistent manner. Many of the most common eddy parameterizations instead rely on the phenomenology of turbulence at a particular scale to parameterize specific components of the tensor. For example, the popular Gent and McWilliams scheme (Gent and McWilliams, 1990; Gent et al., 1995, hereinafter GM) is a parameterization for the eddy tracer fluxes induced by mesoscale baroclinic turbulence, effectively closing only for the vertical fluxes appearing in the bottom row of the EP tensor and only in the limit of large-scale, along-isopycnal flow. The GM parameterization holds particular appeal because it can both be thought of in residual-mean context as introducing an “eddy transport velocity” (offering potential advantages for the numerical implementation of the scheme, e.g. Griffies, 1998; Griffies et al., 1998), and also through its relationship to other downgradient diffusive closures (e.g. Redi, 1982). The latter point has prompted ocean modelers to explore the relationship between the transport coefficients of the GM and Redi parameterizations (e.g. Dukowicz and Smith, 1997; Griffies, 1998; Abernathey et al., 2013; Bachman and Fox-Kemper, 2013), and to develop techniques to ensure that these parameterizations are scale-aware (e.g. Bachman et al., 2016; Pearson et al., 2016) and satisfy appropriate

boundary conditions (e.g. Aiki et al., 2004; Ferrari et al., 2008, 2010).

It is now widely recognized that the GM and Redi transport coefficient must vary both spatially and temporally, though optimal choices for these coefficients remains an open question. Many proposed choices have appeared in the years since the GM and Redi parameterizations were initially developed (Redi, 1982; Gent and McWilliams, 1990; Gent et al., 1995) and concatenated (Griffies, 1998) for practical use. The values of the proposed coefficients have been informed by a variety of methods, including baroclinic instability theory (Visbeck et al., 1997; Killworth, 1997), adjoint modeling (Ferreira et al., 2005), energetic arguments (Cessi, 2008; Eden and Greatbatch, 2008; Marshall and Adcroft, 2010), parcel excursion theory (Fox-Kemper et al., 2008), and direct diagnosis (Bachman and Fox-Kemper, 2013). While each of these proposals has shown promise in replicating key eddy transport characteristics in specific model configurations, their skill at matching diagnosed buoyancy diffusivities has never been compared in a systematic way. In this paper such a systematic comparison will be performed using a suite of idealized models. As the GM parameterization was designed to mimic the restratification and available potential energy extraction of mesoscale baroclinic instability, the basic test case for this comparison will be the spindown of a baroclinically unstable front (e.g. Bachman and Fox-Kemper, 2013).

Included among the list of coefficients in this comparison is an expression for the GM transport coefficient that is inferred using the geometric framework of Marshall et al. (2012). It will be shown that this expression exhibits greater skill at matching the diagnosed buoyancy diffusivities at all times during the baroclinic spindown across the full range of model initial conditions. The goal of this paper will be to highlight the skill of this closure, and in doing so to demonstrate a practical use for the geometric framework and its nontraditional approach to the eddy parameterization problem. This is intended as a possible first step towards a more unified treatment of parameterizing subgridscale eddy fluxes, wherein all terms comprising the EP tensor would be represented in a physically consistent way that conserves energy and momentum.

The outline of this paper is as follows. In Section 2.1 the geometric framework will be reviewed and it will be shown how this leads to a prescription for the GM transport coefficient. The basic theory of downgradient, mesoscale eddy closures is reviewed in Section 2.2, along with the extant scalings for the transport coefficient that are compared using the modeling suite. Section 3 discusses the numerical models used to test the skill of these scalings and presents the results from the comparison. A discussion of the implications of these results, along with concluding remarks, appears in Section 4.

2. Background and theory

2.1. Using the geometric framework to infer an eddy transport coefficient

The “eddy” component of a flow variable is typically defined as the deviation away from some average, and additional advantages are gained when the averaging operation is defined so as to reduce the complexity of the resulting equations of motion. Of particular interest are averaging operations which permit the equations of motion to be rewritten in residual-mean form (e.g. Andrews and McIntyre, 1976; Andrews, 1983; de Szoeke and Bennett, 1993; McDougall and McIntosh, 2001; Young, 2012; Maddison and Marshall, 2013).

Residual-mean theory has previously been used in conjunction with the QG approximation to yield various forms of an eddy flux tensor whose double divergence describes the time tendency (hereafter “eddy tendency”) of QG potential vorticity (e.g. Hoskins et al., 1983; Plumb, 1986; Cronin, 1996) due to turbulence. More recently, this approach has been extended to the hydrostatic Boussinesq primitive equations (Young, 2012; Maddison and Marshall, 2013), where the associated eddy flux tensor still provides information on the eddy tendency of (Ertel) potential vorticity, but appears in the momentum equations instead of the potential vorticity conservation equation. If it is assumed that the buoyancy increases strictly monotonically with height, the resulting equation set can be written in Cartesian coordinates as

$$\frac{D^\# \hat{\mathbf{u}}}{Dt} + f \hat{\mathbf{k}} \times \hat{\mathbf{u}} + \nabla_h p^\# = \mathcal{F} - \nabla_3 \cdot \mathbf{E}, \quad (1)$$

$$\frac{\partial p^\#}{\partial z} = b^\#, \quad (2)$$

$$\nabla_3 \cdot \hat{\mathbf{u}} = 0, \quad (3)$$

$$\frac{D^\# b^\#}{Dt} = \mathcal{B}. \quad (4)$$

123 The averaging operation used to derive (1) - (4) is an ensemble average in buoyancy coordinates (e.g.
 124 Andrews, 1983; de Szoeke and Bennett, 1993; McDougall and McIntosh, 2001; Young, 2012), defined such
 125 that the horizontal components of the Eulerian velocity, (u, v) , are weighted by the isopycnal layer thickness
 126 σ ,

$$(\hat{u}, \hat{v}) = (\overline{\sigma u}, \overline{\sigma v}) / \overline{\sigma}. \quad (5)$$

127 Variables with a superscript $\#$ are defined in terms of the mean depth of an isopycnal surface, as in Young
 128 (2012, equations 59, 73, and 135). The resulting $\hat{\mathbf{u}} = (\hat{u}, \hat{v}, w^\#)$ is known as the residual velocity; ∇_h is
 129 the horizontal gradient operator, ∇_3 is the three-dimensional divergence operator, $D^\# / Dt = \partial / \partial t + \hat{\mathbf{u}} \cdot \nabla_3$
 130 is the material derivative following the residual velocity, f is the Coriolis parameter, \mathcal{F} represents external
 131 momentum forcing, and \mathcal{B} represents external buoyancy forcing.

132 Henceforth the quasi-geostrophic limit will be considered, the overbar will refer to an appropriate aver-
 133 age at fixed height, and primes will indicate deviations from this average.¹ The buoyancy frequency will be
 134 denoted by

$$N_0(z) = \left(\partial \bar{b} / \partial z \right)^{1/2}. \quad (6)$$

135 All eddy forcing is wrapped into the column-wise divergence of \mathbf{E} , the 3×3 ‘‘Eliassen–Palm flux tensor’’
 136 (hereinafter EP tensor, e.g. Maddison and Marshall, 2013), so named in order to highlight its relevance to
 137 the eddy transport of potential vorticity. At the QG level of approximation, because the eddy tendency of
 138 potential vorticity is given by the double divergence of \mathbf{E} , one may freely add rotational terms (‘‘gauges’’) to
 139 either the rows or columns of \mathbf{E} . Here the gauge is chosen so that the form of \mathbf{E} to be considered in this
 140 paper is (Plumb, 1986)

$$\mathbf{E} = \begin{bmatrix} -M + P & N & 0 \\ N & M + P & 0 \\ -S & R & 0 \end{bmatrix}, \quad (7)$$

¹For details of how this averaging is performed between density and Cartesian coordinates, the reader should refer to Young (2012). Maddison and Marshall (2013) discuss the mathematical properties required of the averaging operator in order for the subsequent results to hold, and derive a coordinate-invariant form of the residual-mean equations. It is shown in Appendix A how the GM parameterization arises in the context of this averaging at both the unapproximated and quasigeostrophic levels.

141 where

$$M = \frac{\overline{v'^2 - u'^2}}{2} \quad (8a)$$

$$N = \overline{u'v'} \quad (8b)$$

$$P = \frac{\overline{b'^2}}{2\mathcal{N}_0^2} \quad (8c)$$

$$R = \frac{f}{\mathcal{N}_0^2} \overline{u'b'} \quad (8d)$$

$$S = \frac{f}{\mathcal{N}_0^2} \overline{v'b'}. \quad (8e)$$

142 One benefit of writing the eddy stresses as part of a tensor is that it allows the underlying geometric
 143 nature of the eddy fluxes to be clarified. Marshall et al. (2012) used this geometry to develop relationships
 144 between the eddy flux amplitudes, orientations, and anisotropies that are not readily apparent through basic
 145 Reynolds averaging. A particularly useful result emerging from their geometric formalism is a bound on the
 146 magnitude of the elements of \mathbf{E} ,

$$M^2 + N^2 + P^2 + \frac{\mathcal{N}_0^2}{2f^2} (R^2 + S^2) \leq 2E^2, \quad (9)$$

147 where the vertical components of \mathbf{E} are weighted by the inverse square of the Prandtl ratio, f/\mathcal{N}_0 . The
 148 key component of this bound is the eddy energy, $E = K + P$, which is the sum of the eddy kinetic energy
 149 $K = \frac{1}{2} \overline{\mathbf{u}'_h \cdot \mathbf{u}'_h}$, and QG-approximated eddy potential energy, P . The utility of (9) is that it allows one to
 150 express the inherent geometry of the EP tensor through its individual components. In terms of developing
 151 an eddy parameterization, this bound means that each component comprising \mathbf{E} can be written as a function
 152 of the eddy energy (see Marshall et al., 2012, equation 16).

153 Of special interest to the eddy parameterization problem are the lateral buoyancy fluxes R and S , which
 154 have historically been given a special role in mesoscale eddy closures owing in large part to the success of
 155 the GM parameterization. Marshall et al. (2012) showed that the geometric formalism can be used to derive
 156 a scalar eddy transport coefficient for a downgradient buoyancy closure of the form

$$\overline{\mathbf{u}'_h b'} = -\kappa_G \nabla_h \bar{b}, \quad (10)$$

157 which, using the energetic bound on the buoyancy flux magnitude, can be re-arranged to imply a value for
 158 the GM transport coefficient,

$$\kappa_G = \alpha E \frac{\mathcal{N}_0}{|\nabla_h \bar{b}|}. \quad (11)$$

159 Here the subscript $_G$ will differentiate this scaling from others which will be introduced later on. In (11)
 160 the dimensionless parameter α , which measures the relative magnitudes of the eddy buoyancy fluxes to the
 161 eddy kinetic and potential energies (Marshall et al., 2012), is constrained in magnitude such that $|\alpha| \leq 1$. A

significant advantage of the closure (11) is that once the eddy energy and mean stratification are known, the only uncertain parameter is α , which is nondimensional. Furthermore, because the expression for κ_G follows directly from the EP tensor geometry, as long as α is bounded away from zero the scaling $\kappa_G \sim E\mathcal{N}_0/|\nabla_h \bar{b}|$ must hold.

The presence of E in (11) suggests that larger, more energetic eddies are capable of more efficient mixing, consistent with extant theories (e.g. Prandtl, 1925; Green, 1970; Stone, 1972) and turbulence closures (e.g. Mellor and Yamada, 1982; Gaspar et al., 1990; Rodi, 1993; Cessi, 2008; Eden and Greatbatch, 2008; Marshall and Adcroft, 2010; Bachman and Fox-Kemper, 2013; Jansen et al., 2015) in which the transport coefficient depends on the eddy kinetic energy. Note, however, that E also includes a contribution from the eddy potential energy, P , which is not included in previous closures. The skill of the proposed scaling in (11) has heretofore been untested.

2.2. Parameterization of eddy tracer fluxes

The scaling (11) is a useful result because it specifies the physical dimensional parameters, such as the eddy energy and buoyancy frequencies, which govern the lateral buoyancy mixing rate. However, it has long been argued that eddy transport in the interior of the ocean is principally oriented along isopycnal surfaces,² so that a *scalar* flux-gradient relationship is insufficient to describe the motion in z -coordinate models so long as the neutral and z -surfaces do not coincide. Rather, the likely misalignment of these surfaces requires that the directional transport be described by a second-rank eddy transport *tensor* whose transformation properties follow the usual tensor calculus rules (e.g. Redi, 1982; Griffies, 2004; Aris, 2012). Here the basic underpinnings of downgradient eddy parameterizations are reviewed, and in particular it will be shown how in the large-scale, small isopycnal-slope limit the lateral fluxes associated with the eddy transport tensor can be approximated by a scalar transport coefficient, facilitating testing of closures like (11).

A common approach in the development of eddy parameterizations is to assume a linear flux-gradient relationship (e.g. Taylor, 1921; Vallis, 2006) between the subgridscale eddy fluxes and the gradient of a resolved tracer, τ ,

$$\overline{\mathbf{u}'\tau'} = -\mathbf{K} \cdot \nabla \bar{\tau}, \quad (12)$$

where \mathbf{K} is a 3×3 eddy transport tensor describing the net, directional rate by which eddies advect and diffuse the tracer. Inherent within the flux-gradient relationship is an assumption of locality, where the unresolved turbulence is able to mix fluid parcels of differing tracer concentration based on their close proximity to each other (hence the appearance of the gradient operator in (12)). As such, while this approach has been successful for parameterizing eddy buoyancy transport (e.g. Bachman and Fox-Kemper, 2013), it is unclear whether it is appropriate for parameterizing eddy momentum transport, where nonlocal pressure effects are also capable of redistributing momentum (e.g. Harcourt, 2015).

Nonetheless, successful and popular parameterizations such as GM and Redi rely on the flux-gradient relationship to develop closures for the tracer budgets, leaving the unresolved momentum fluxes to be handled separately. These parameterizations are completed by specifying a turbulent, scalar transport coefficient, along with expressions for each of the nine elements of \mathbf{K} to represent the anisotropy of the eddy transport.

²Fox-Kemper et al. (2013) describe the transport as being along “minimal-disturbance” surfaces, which is a blanket term used to describe a number of different thermodynamic variables whose perturbations are minimized by adiabatic motions (e.g. McDougall, 1987; Young, 2010; Nycander, 2011). The specific variable and terminology depends on the level of thermodynamic accuracy required; in this paper we will use “isopycnal” surfaces due to the special role of b in residual-mean theory.

198 For example, assuming an along-isopycnal flow in the QG limit of small isopycnal slopes, the GM and Redi
 199 parameterizations can be jointly expressed as

$$\mathbf{K}_{GM/Redi} = \begin{bmatrix} \kappa_R & 0 & (\kappa_R - \kappa_{GM}) S_x \\ 0 & \kappa_R & (\kappa_R - \kappa_{GM}) S_y \\ (\kappa_R + \kappa_{GM}) S_x & (\kappa_R + \kappa_{GM}) S_y & \kappa_R (S_x^2 + S_y^2) \end{bmatrix}, \quad (13)$$

200 where κ_R is the Redi diffusivity, κ_{GM} is the GM transport coefficient, and $(S_x, S_y) = -\nabla_h \bar{b} / N_0^2$ are the
 201 isopycnal slopes (Griffies, 1998). A significant amount of research has gone into studying the structure of
 202 this tensor (Plumb, 1979; Plumb and Mahlman, 1987; Redi, 1982; Middleton and Loder, 1989; Gent and
 203 McWilliams, 1990; Gent et al., 1995; Dukowicz and Smith, 1997; Griffies, 1998), the distinction between
 204 the eddy stirring and mixing it induces (Müller and Garrett, 2002; Bachman et al., 2015), and generalizations
 205 into horizontally anisotropic eddy transport (Smith and Gent, 2004).

206 In writing (13), the assumption of layer-wise flow places strong constraints on the structure of the eddy
 207 transport tensor, in effect specifying the anisotropy between the horizontal and vertical directions and absolv-
 208 ing the modeler from having to specify $\mathbf{K}_{GM/Redi}$ element by element. Though a method exists for diagnosing
 209 the full tensor (e.g. Bachman and Fox-Kemper, 2013; Bachman et al., 2015), the additional degrees of free-
 210 dom in a 3×3 tensor make diagnosis of the associated transport coefficients significantly more complicated
 211 than if a scalar flux-gradient relationship like (10) were used instead. Inspection of (13) reveals that in the
 212 small-slope limit the diagnosis problem becomes significantly easier if it is assumed that the GM transport
 213 coefficient and Redi diffusivity are equal, so that

$$\kappa_R = \kappa_{GM}. \quad (14)$$

214 In this case all off-diagonal terms of the horizontal fluxes become zero, so that the horizontal buoyancy flux
 215 can be well-approximated by

$$\overline{\mathbf{u}'_h \tau'} = -\kappa_{GM} \nabla_h \bar{\tau}. \quad (15)$$

216 It has been shown previously that (14) is unlikely to hold except in special circumstances. For example,
 217 Smith and Marshall (2009) showed that (14) is only possible assuming that $\beta = \partial f / \partial y$ is negligible, and
 218 Dukowicz and Smith (1997) used stochastic turbulence theory to show that (14) holds only if κ_R and κ_{GM}
 219 are isotropic and constant along isopycnal surfaces. This necessarily cannot be true everywhere in order
 220 to satisfy zero-flux boundary conditions at the ocean surface and bottom, which has given rise to various
 221 methods of tapering the GM/Redi transport to zero near the ocean boundaries (e.g. Griffies, 2004; Ferrari
 222 et al., 2008, 2010). However, it is important to note that the results of Dukowicz and Smith (1997) only
 223 require the coefficients to be isotropic and constant in the two-dimensional, along-isopycnal plane. In the
 224 QG limit where the isopycnal slopes are nearly flat, this implies that $\kappa_R \approx \kappa_{GM}$ along horizontal planes,
 225 permitting the diffusivities to vary in the vertical and satisfy the appropriate boundary conditions *while still*
 226 *remaining equal at all vertical levels*.

227 It is possible to design a basic model configuration to replicate the circumstances in which (14) is ex-
 228 pected to hold. Indeed, Bachman and Fox-Kemper (2013) performed a suite of simulations using a zonally
 229 reentrant channel on the f -plane with basic stratification similar to that of the Eady (1949) model, and found
 230 that $\kappa_R \approx \kappa_{GM}$ at all vertical levels, so that the lateral eddy transport can be approximately determined by a
 231 scalar transport coefficient as in (10). Their idealized model configuration thus provides an excellent means
 232 of testing various scalings for the GM coefficient which have appeared in previous literature.

2.3. Extant expressions for the GM transport coefficient

Various expressions have been proposed for the value of the GM coefficient (e.g. Visbeck et al., 1997; Bryan et al., 1999; Ferreira et al., 2005; Eden and Greatbatch, 2008; Marshall et al., 2012; Abernathy et al., 2013; Bachman and Fox-Kemper, 2013), along with methods to taper it near the vertical boundaries (e.g. McIntosh and McDougall, 1996; Treguier et al., 1997; McDougall and McIntosh, 2001; Ferrari et al., 2008, 2010). While sensitivity to changing the GM transport coefficient has been demonstrated in global-scale GCMs (e.g. Danabasoglu and Marshall, 2007; Eden et al., 2009; Farneti and Gent, 2011), the relative skill of these proposed coefficients has not been compared directly using idealized, eddy-resolving models. In this paper we perform such a comparison by mimicking the approach of Bachman and Fox-Kemper (2013), which is to create a suite of idealized hydrostatic Eady-like channel models in which the eddy fluxes can be explicitly diagnosed. The advantage of using this “eddy parameterization challenge suite” is that it allows the modeler to vary the basic model configuration in a systematic way to determine whether the proposed scalings for κ_{GM} are accurate across a wide range of parameter space.

In this testing suite, a flux-gradient relation of the form (15) is inverted for an ensemble of tracers to obtain a best estimate for the GM transport coefficient. This estimate is compared against the above scalings, which are calculated directly using model diagnostics of E , K , N_0^2 , and so on. The accuracy of the scalings is compared at regular intervals in time during the frontal spindown and across a range of stratification parameters.

In particular, we are interested in testing the accuracy of the coefficient obtained using the geometric framework,

$$\kappa_G = \alpha E \frac{N_0}{|\nabla_h \bar{b}|}, \quad (16)$$

against four others. These are:

i) The transport coefficient introduced in Visbeck et al. (1997),

$$\kappa_v = \alpha_v L^2 \sigma, \quad (17)$$

where α_v is a nondimensional tuning parameter, L is an eddy length scale, and $\sigma = f Ri^{-1/2}$ is the Eady growth rate written as a function of the balanced Richardson number $Ri = N_0^2 f^2 / |\nabla_h \bar{b}|^2$. Visbeck et al. (1997) suggested to set $L = \max(\Delta, L_D, L_Z)$, where Δ is the horizontal grid spacing of the model, $L_D = N_0 H / |f|$ is the external Rossby radius (e.g. Stone, 1972) based on the total ocean depth H , and L_Z is the width of the “baroclinic zone” (e.g. Green, 1970), defined as the region where the local Eady growth rate exceeds 10% of the maximum growth rate of the field.

Because the initial stratification of the models described in Section 3 is spatially constant, the width of the baroclinic zone by the above definition would be the entire simulation domain, making it an unsuitable choice for L . In each model the grid spacing is set as $\Delta x = L_D$, yielding an eddy length scale $L = N_0 H / f$. The tuning parameter is set to the value originally proposed by Visbeck et al. (1997), $\alpha_v = 0.015$. Note also that κ_v is very similar to the “simplified closure” suggested by Eden and Greatbatch (2008), who instead chose L as the minimum of the Rossby radius and the Rhines scale; for the f -plane simulations conducted here, they are equivalent aside from the value of the tuning parameter.

268 ii) A transport coefficient developed using parcel excursion theory and derived from the work of Fox-Kemper
 269 et al. (2008),

$$\kappa_F = 0.06 \frac{N_0^2 H^2}{f}. \quad (18)$$

270 A critical assumption used in deriving this coefficient is that the eddy velocity scales with the thermal wind
 271 shear, resulting in a final scaling for κ_F that is independent of the eddy energies. Note that, although the
 272 Fox-Kemper et al. (2008) eddy parameterization itself was constructed to mimic restratification by mixed
 273 layer baroclinic eddies, no part of its derivation is specific to mixed layer dynamics. Therefore, the inferred
 274 value of κ_F is suitable to be tested against the other coefficients presented here.

275 iii) The closure suggested by Eden and Greatbatch (2008),

$$\kappa_E = K^{1/2} L, \quad (19)$$

276 where the mixing length L is chosen as the minimum of the Rossby radius and the Rhines scale. In devel-
 277 oping this closure, Eden and Greatbatch (2008) suggested an additional prognostic equation to solve for K ,
 278 where the result would then be fed into the calculation of κ_E . Though no such prognostic equation exists for
 279 the models in Section 3, a major advantage of the eddy challenge suite is that K can be diagnosed directly.

280 iv) A “best-fit” transport coefficient diagnosed by Bachman and Fox-Kemper (2013),

$$\kappa_B = 0.32 Ri^{-0.31} \frac{N_0^2 H}{|\nabla_h \bar{b}|} K^{1/2}. \quad (20)$$

281 The dependence of κ_B on the eddy kinetic energy was theorized using Lagrangian parcel displacements
 282 (e.g. Taylor, 1921; Plumb, 1979; Plumb and Mahlman, 1987), and the nondimensional coefficients were
 283 diagnosed using nearly identical models as those described in Section 3.

284 3. Diagnosis in the Eady model

285 3.1. Model setup

286 A series of simulations have been conducted using the MIT General Circulation Model (Marshall et al.,
 287 1997) to diagnose eddy flux statistics to use in comparing the scalings for κ_{GM} listed previously. Each
 288 simulation features a zonally elongated, flat-bottom channel with $(x, y, z) = (600, 100, 50)$ gridpoints, which
 289 is periodic in the zonal direction and bounded meridionally by vertical walls. The simulations are set up with
 290 no external forcing and an initial stratification matching the Eady (1949) problem, with spatially uniform
 291 vertical and lateral density gradients. These models use a linear equation of state, where the density is
 292 only a function of potential temperature. The initial stratification parameters, $\mathcal{M}^2 = \partial \bar{b} / \partial y$ and N_0^2 , are
 293 varied around a set of values informed by the simulations of Jones et al. (2015) using the Southern Ocean
 294 State Estimate (Mazloff et al., 2010), and are set as $\mathcal{M}^2 = \{5 \times 10^{-10}, 10^{-9}, 2 \times 10^{-9}, 4 \times 10^{-9}\} \text{ s}^{-2}$ and
 295 $N_0^2 = \{1 \times 10^{-5}, 2 \times 10^{-5}, 4 \times 10^{-5}, 8 \times 10^{-5}\} \text{ s}^{-2}$. This amounts to sixteen simulations in total, with each

differing according to the initial stratification parameters used. The horizontal grid resolution is set equal to the internal deformation radius for the initial state of that simulation, $\Delta x = \frac{N_0 H}{|f|}$, and the vertical resolution is set at 80 m, for a total depth of $H = 4000$ m. The simulations are conducted on an f -plane with $f = -1.25 \times 10^{-4} \text{ s}^{-1}$. In all, these dimensional parameters and the zonal channel configuration represent an idealized Southern Ocean, which is intended as a lead-in to future work. Each simulation uses modified Leith viscosity (Fox-Kemper and Menemenlis, 2008) with nondimensional scaling factor $\Lambda = 1$.

The zonal channel models and averaging used in these simulations are similar to those used in Bachman and Fox-Kemper (2013), except that in these simulations the horizontal density gradient is initially uniform everywhere rather than being concentrated at an isolated front. The technique used to diagnose the eddy transport coefficient is an adapted version of the multiple-tracers inversion method used in that work.

Here an ensemble of twenty passive tracers is initialized in each model, where the initial profile of each tracer varies sinusoidally throughout the domain. This initial configuration is sufficient to keep the tracer gradients from becoming aligned through the duration of each simulation, which would cause the tracer inversion method to fail. The initial tracer profiles are set according to the convention in Bachman et al. (2015, equation 32). Each tracer is assumed to satisfy its own tensor flux-gradient relation of the form (12); assuming that the properties of the eddy transport tensor \mathbf{K} are a function of the turbulence itself and not the tracer, one may then write the ensemble of flux-gradient relations in matrix form,

$$\overline{u'_i \tau'_\pi} = -K_{ij} \nabla_j \bar{\tau}_\pi, \quad (21)$$

where i and j are row and column indices and π is the tracer index. For a 3×3 transport tensor the diagnosis of \mathbf{K} is underdetermined and will not yield a unique solution if the number of tracers $\pi < 3$. Choosing $\pi = 3$ tracers makes it possible to perform a regular matrix inversion on $\nabla_j \bar{\tau}_\pi$ to solve for \mathbf{K} , but the solution is not guaranteed to be accurate because there can be a large amount of variability in the tracer fluxes and gradients along the length of the channel which is masked by the averaging operation. Therefore, it is appropriate to initialize $\pi > 3$ tracers and pseudoinvert (e.g. Eldén, 1982) the tracer gradient matrix, in which case the obtained solution for \mathbf{K} becomes the best fit to the eddy statistics in the least-squares sense. In essence, one combines a large number of eddy realizations (i.e. a long channel) with a large number of tracers to create a very large statistical ensemble with which to estimate the diffusivities. Using this technique, Bachman and Fox-Kemper (2013) found less than 7% error between buoyancy fluxes diagnosed from the model and the “reconstructed” buoyancy fluxes,

$$\overline{\mathbf{u}' b'}_{rec} = -\mathbf{K} \cdot \nabla \bar{b}. \quad (22)$$

As in Bachman and Fox-Kemper (2013), the averaging operation is a zonal average along the length of the channel; because of this averaging, all zonal gradients of averaged quantities become zero. Furthermore, the QG approximation of small isopycnal slopes predicts that the off-diagonal terms of the now- 2×2 transport tensor are negligibly small. In all, this leaves a much simplified ensemble flux-gradient relation,

$$\overline{v' \tau'_\pi} = -\kappa \frac{\partial \bar{\tau}_\pi}{\partial y}, \quad (23)$$

which can now be inverted for a scalar κ . The zonally-averaged tracer fluxes and tracer gradients each form a vector *at every point on the yz -plane*, and κ is determined by taking the dot product of the eddy flux vector with the pseudoinverted tracer gradient vector. The overall value of κ for that time is taken as the domain average of these solutions. A schematic of the model setup and inversion procedure is shown in Figure 1.

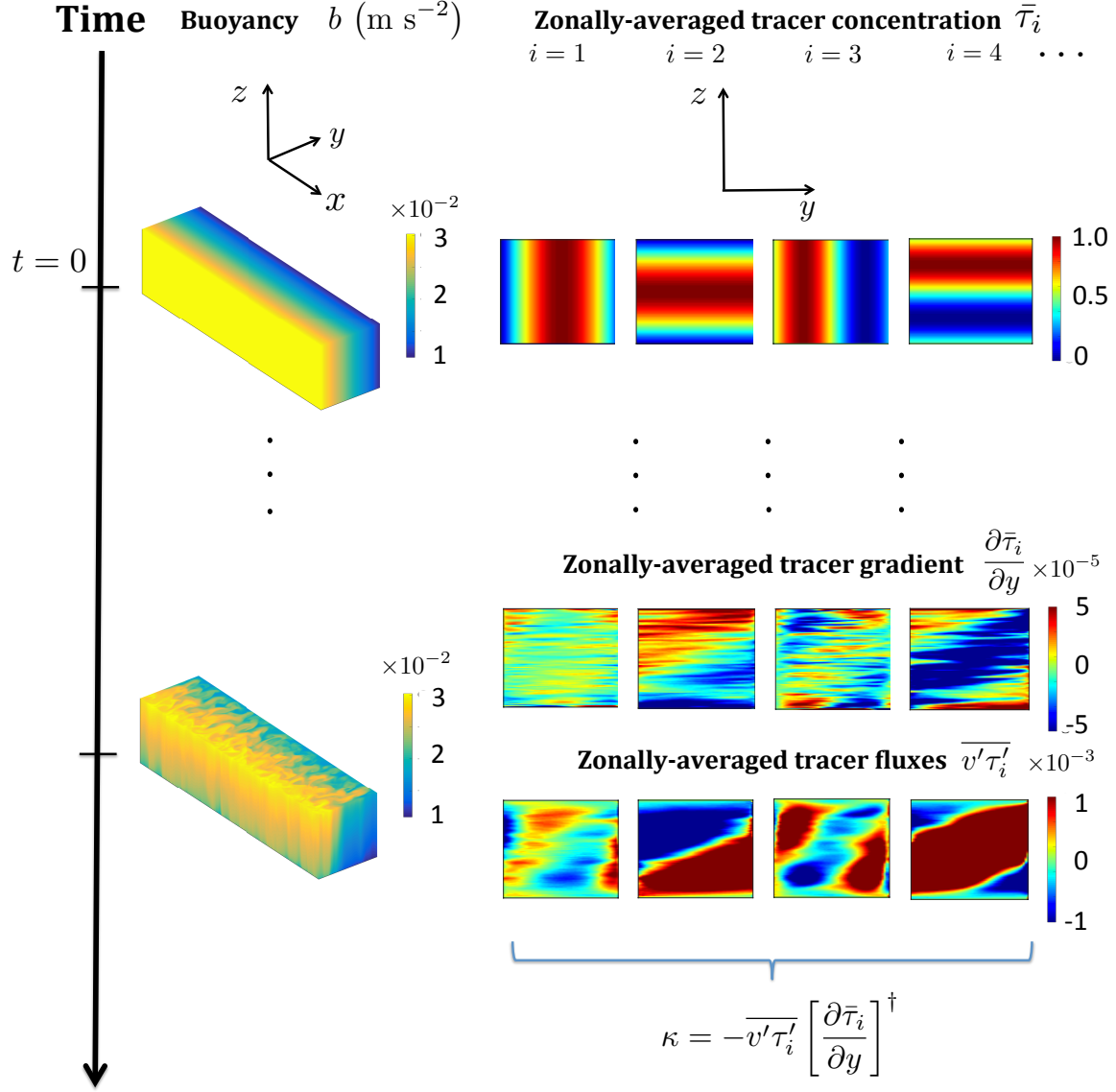


Figure 1: Schematic of Eady model configuration and diagnostic procedure. The shear and stratification at time $t = 0$ are constant, and the initial tracer profiles vary sinusoidally in y and z as in Bachman and Fox-Kemper (2013). At later times after the front goes baroclinically unstable, the tracer concentrations are zonally averaged, their meridional gradients and eddy fluxes are calculated, and a solution for κ is obtained by pseudoinverting (23) at each point on the yz -plane. The overall value for κ at each output interval is taken as the domain average of these solutions. In the inset panels the tracer gradients and fluxes may vary beyond the given color scale, but the color limits are chosen to be suitable for all tracers shown. In the buoyancy plots the aspect ratio of the domain has been stretch to illustrate both the along-channel and vertical aspects of the turbulence; the actual density surfaces in the simulations are nearly flat.

Time-averaged output from each simulation is written out once every ten days of model time. The velocity fields are zonally averaged to diagnose the eddy kinetic energy, K , every one hundred days of model time, and the simulations are stopped approximately one thousand days after the domain-averaged K appears to have reached its peak.

3.2. Comparison of transport coefficients

Figure 2 shows the diagnosed κ obtained by pseudoinverting (23) plotted against the five scalings listed in Section 2.2. Each point on the plot represents the domain-averaged value of κ (both the pseudoinverted solution and scalings) at each output time for all sixteen simulations. Here we have restricted the axes to show only values of $\kappa > 10$ and values diagnosed before the saturation time (here defined to be when E reaches 25% of its maximum value). The former restriction avoids meaningless noise in the diagnosis during the early spinup phase, when the covariance between the tracer and buoyancy fluxes needed for the tracer inversion method to work have not yet been established (some artifacts from the spinup appear as outliers in panels (a), (c), and (d)). The latter restriction avoids interactions with the lateral boundaries, which also disrupt the covariance between the fluxes and lead to inaccuracy in the diffusivity diagnoses. Because the numerical models simulate eddy spinup from an initially laminar flow, the diffusivity grows over time as the eddies become nonlinear, and can range over multiple orders of magnitude during the same simulation (Figure 3). Because the simulations progress through different turbulence regimes (linear growth, nonlinear spinup, and saturation), it is especially challenging for a scaling to demonstrate skill at all times.

For the Marshall et al. (2012) form of the transport coefficient diagnosed here, a constant value of $\alpha = 0.2$ is used, a choice which is discussed in Section 3.3. This scaling is shown in panel (a), and demonstrates excellent skill at matching the diagnosed diffusivity at all pre-saturation times. The other panels in Figure 2 compare the other scalings listed in Section 2.1. The other two scalings which use at least part of the eddy energy (Bachman and Fox-Kemper (2013) and Eden and Greatbatch (2008), which are shown in panels (d) and (e) and are dependent only on K) are skillful in the large-diffusivity regime during nonlinear spinup, but less so at earlier times. The Visbeck et al. (1997) and Fox-Kemper et al. (2008) scalings, which are shown in panels (c) and (f) and do not depend on any type of eddy energy, fail to demonstrate skill at any time and do not trend with the diagnosed diffusivity at all.

3.3. Dependence of κ_G on eddy energy and α

These comparisons indicate that the eddy energy is a fundamental parameter in determining the skill of the eddy closure, but thus far it is not clear to what degree this skill is dependent on the *type* of eddy energy. This is a key difference between the Marshall et al. (2012) scaling and the Bachman and Fox-Kemper (2013) and Eden and Greatbatch (2008) scalings, where the former relies on the total eddy energy and the latter two on the eddy kinetic energy. Figure 4 shows the time evolution of E and the ratio K/P for all simulations. Like the diffusivity shown in Figure 3, E grows in time until the eddy energy reaches saturation. This is consistent with (11), where if the change in α and the stratification parameters over time is relatively small, then E must generally trend with time in the same way as κ . Panel (b) of this figure shows that K/P tends to be less than one after the linear growth phase of the simulations, and in some cases reaches as low as 0.1. Upon saturation this ratio tends to be about 0.8 across all simulations. These results suggest that P contributes non-negligibly to the total eddy energy.

To investigate whether the greater skill of the Marshall et al. (2012) scaling is due to the inclusion of P or due to the functional form of the parameterization itself, each of these parameterizations is plotted against the diagnosed diffusivity, but with a different type of eddy energy substituted in place of the original. That is, we plot

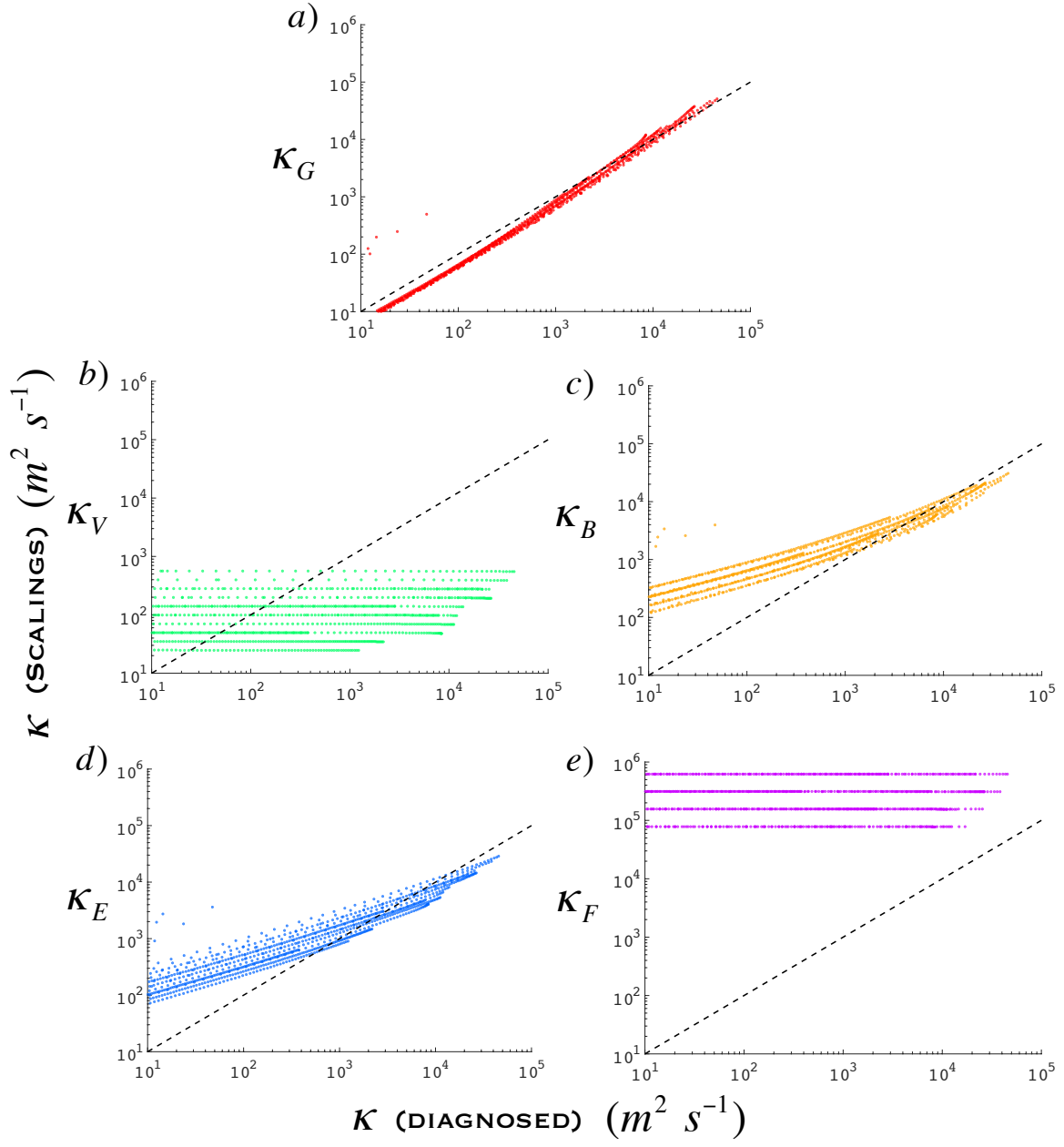


Figure 2: Scatter plots of domain-averaged scalings at each output interval, plotted for all sixteen simulations. The diffusivity diagnosed by the pseudoinversion is plotted along the x-axis, and the scalings are plotted along the y-axis in each panel. Shown here are the scalings from (a) Marshall et al. (2012) with $\alpha = 0.2$, (b) Visbeck et al. (1997), (c) Bachman and Fox-Kemper (2013), (d) Eden and Greatbatch (2008), and (e) Fox-Kemper et al. (2008). The diagonal, dashed black line represents perfect agreement between the diagnosed diffusivity and the scaling.

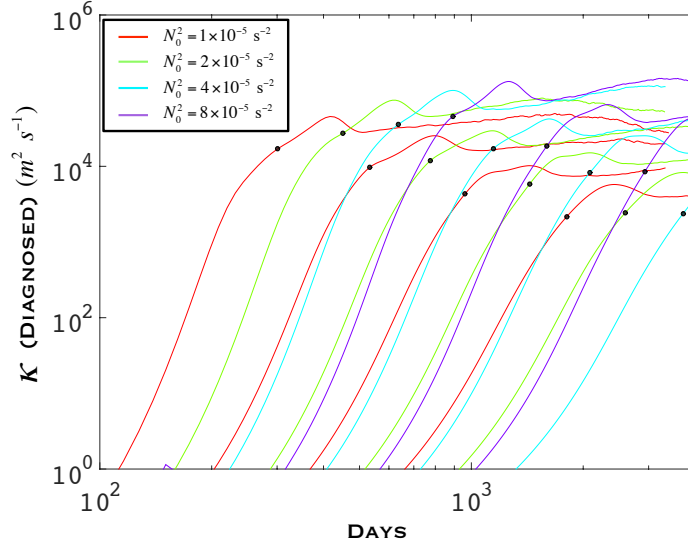


Figure 3: Domain-averaged diffusivity, diagnosed by the pseudoinversion, plotted as a function of time. The shading of the lines differentiates simulations with different values of the initial N_0^2 . The diffusivity grows in time until the eddy energy reaches saturation, which is indicated by the black dots. κ can vary by up to five orders of magnitude over the course of each simulation, posing a challenge for prospective scalings.

$$\kappa_G = \alpha \chi \frac{N_0}{|\nabla_h \bar{b}|} \quad \kappa_E = \chi^{1/2} L \quad \kappa_B = 0.32 Ri^{-0.31} \frac{N_0^2 H}{|\nabla_h \bar{b}|} \chi^{1/2}, \quad (24)$$

for each of $\chi = \{E, K, P\}$. Figure 5 shows that switching between the different eddy energies results in no significant change in how the parameterizations vary with the diagnosed diffusivities. This implies that the main reason for the skill of the Marshall et al. (2012) parameterization is due to its functional form, which is constrained by the geometric formalism in Section 2.1.

The principal advantage of pursuing a parameterization using the geometric formalism in Section 2.1 is that all dimensional terms in the expression for κ_G are explicitly specified, and the only remaining unknown is the nondimensional coefficient α . While the bound $|\alpha| \leq 1$ provides a useful constraint on the magnitude, no parameterization currently exists to capture how α varies with time and the properties of the mean flow, and a skillful closure should attempt to replicate this sensitivity as best as possible.

A major challenge in parameterizing α is that it is not clear in which “state” (growing, decaying, in force-dissipative equilibrium, etc.) subgridscale eddies should be considered in GCMs. Previous studies have shown that emergent scaling laws may differ *for the same basic model configuration* depending on whether the eddy statistics are gathered during nonlinear spinup (e.g. Bachman and Fox-Kemper, 2013), after saturation (e.g. Fox-Kemper et al., 2008), or in statistical equilibrium (e.g. Lee et al., 1997; Eden, 2010, 2011; Bachman and Taylor, 2016). Figure 6 shows α diagnosed directly from the simulations, which varies significantly in time both before and after eddy energy saturation. In these simulations the range of α tends to consistently be between 0 and 0.8, peaking just before saturation. If α is chosen to be constant

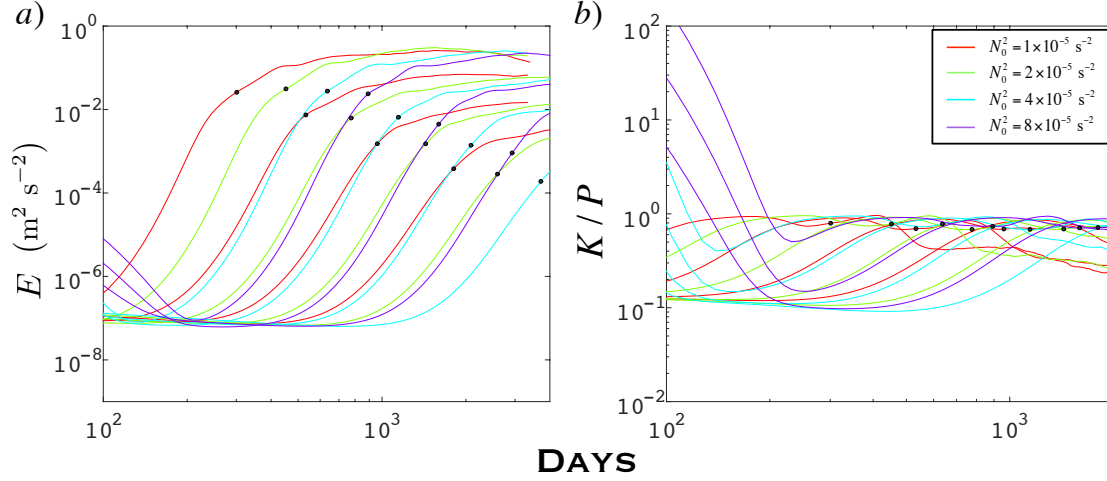


Figure 4: (a) Domain-averaged eddy energy, E , plotted as a function of time for all simulations. The trend mirrors that of the diagnosed diffusivity, growing in time until it reaches saturation (black dots). (b) Ratio of K and P . Because this ratio tends to be less than one, the contribution of P to the eddy energy is non-negligible.

for a parameterization, three obvious choices emerge: (i) the peak value of 0.8, (ii) the value at saturation of 0.7, or (iii) a long-term, equilibrated value of 0.2. Based on Figure 6, option (i) represents a transient state that occurs only for a brief time window, and it is not clear whether there is a physical basis for why $\alpha \approx 0.7$ at saturation in all simulations in option (ii). Therefore, we provisionally recommend the value of $\alpha = 0.2$ in option (iii), which is consistent with the magnitude of related geometric parameters diagnosed in the simulations of Marshall et al. (2012). The result of using this choice for α is shown in Figure 2 to be skillful even in the pre-saturation phase.

The idealized, unforced simulations described in this paper are meant to provide a simple test bed with which to evaluate eddy parameterizations. While these simulations are useful for investigating how the magnitude of eddy transport depends on dimensional parameters such as the eddy energy and buoyancy gradients, it is not clear whether diagnosed values of unknown parameters such as α are meaningful in the context of climate models. It is possible that the equilibrated value of α depends on other factors (such as external forcing, boundary dissipation, bathymetry, etc.) which vary in space and time. A comprehensive study of how to parameterize α is beyond the scope of this paper.

4. Conclusions

In this paper a suite of idealized numerical simulations has been used to compare the skill of several previous proposals for the eddy transport coefficient for the Gent and McWilliams (1990) parameterization. The skill of each proposal was measured by comparing its predicted coefficient against a transport coefficient diagnosed through a multiple-tracers inversion method (e.g. Bachman and Fox-Kemper, 2013; Bachman et al., 2015) at each model output time. Each simulation in the suite used a unique initial value for the lateral and vertical buoyancy gradient, with the initial flow configuration set to mimic that of the Eady (1949) problem. Sixteen simulations were carried out in total.

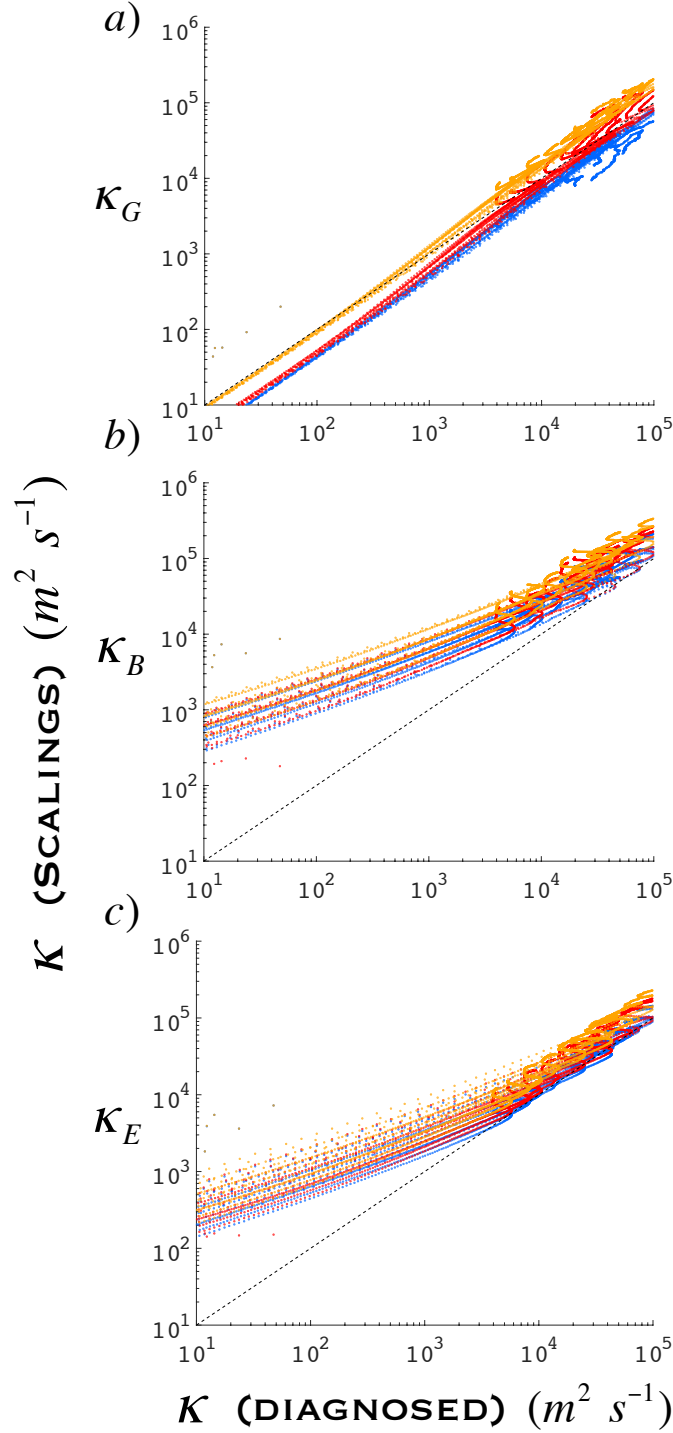


Figure 5: Scatter plots of domain-averaged scalings at each output interval, plotted for all sixteen simulations. The diffusivity diagnosed by the pseudoinversion is plotted along the x -axis, and the scalings are plotted along the y -axis in each panel. Shown here are the scalings from (a) Marshall et al. (2012) with $\alpha = 0.2$, (b) Bachman and Fox-Kemper (2013), and (c) Eden and Greatbatch (2008). The different types of eddy energy used in each parameterization are differentiated by color: red indicates the total eddy energy, E ; orange indicates the eddy kinetic energy, K ; blue indicates the eddy potential energy, P . These results are plotted on the same panel to emphasize that swapping energy types makes little difference aside from rescaling by a small, nearly constant factor, but otherwise does not affect the relationship between diagnosed and parameterization diffusivities.

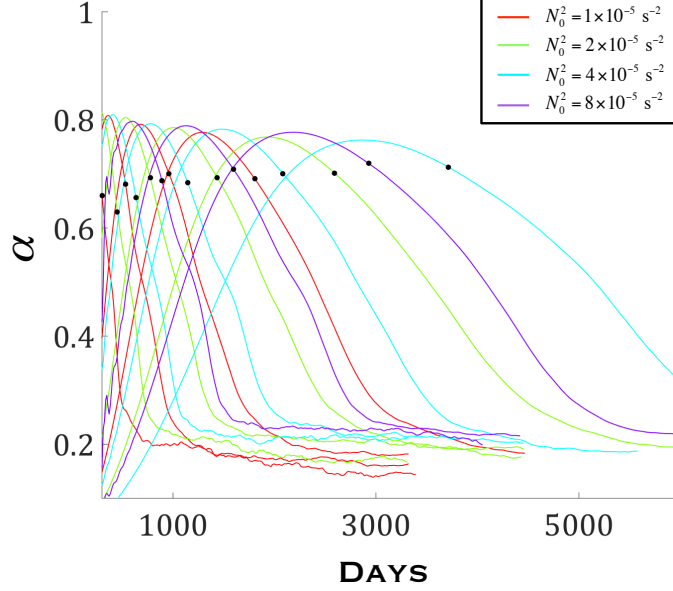


Figure 6: Time evolution of α for all simulations. The black dots indicate the time of eddy energy saturation.

Among the scalings shown in this comparison, we have highlighted the scaling of Marshall et al. (2012) due to its high skill at predicting the eddy transport coefficient across all model output times and simulations in the suite. This scaling arises through an eddy parameterization framework inspired by residual-mean theory, wherein all of the subgridscale eddy forces are isolated to the horizontal momentum equations. One of the key advantages that arise through this framework is the emergence of a bound on the norm of the Eliassen–Palm tensor, \mathbf{E} , which constrains the magnitude of each tensor element. When this concept is applied as part of downgradient diffusive closure, the form of the resultant transport coefficient, κ_G , is also constrained, and the magnitude of the associated parameter α is bounded such that $|\alpha| \leq 1$.

The dependence of κ_G on the eddy energy is similar to that of previous closures (e.g. Eden and Greatbatch, 2008; Bachman and Fox-Kemper, 2013), though both the type of eddy energy (total for the Marshall et al. (2012) closure, and kinetic for the others), its exponent, and the other parameters multiplying the eddy energy differ. To investigate the importance of the energy type in these closures, each parameterization was evaluated using all three types of eddy energy (total, kinetic, and potential). The skill of these closures at matching the diagnosed transport coefficients showed little sensitivity to the energy type. Because one of the primary challenges in using these parameterizations is determining the eddy energies, this may have strong implications on the optimal way to implement these parameterizations in a GCM. For example, in QG flows the relative magnitudes of the eddy kinetic and potential energies can be expressed in terms of the nondimensional Burger number, $Bu = N_0 H / fL$, as

$$K = Bu^2 P. \quad (25)$$

For models whose subgridscale dynamics are QG so that $Bu = O(1)$, K and P are of the same order, so that

if one assumes that their relationship stays relatively fixed as other flow parameters change (e.g. rotation, shear, stratification, etc.), it may be justified to forego two separate energy equations in favor of only one. Furthermore, because prognostic equations for the eddy energies are uncommon in GCMs, this implies that it may be justifiable to calculate whichever type of energy is easiest and simply use that in the parameterization.

It is cautioned, however, that the lack of sensitivity to swapping energy types may be due in part to the simplicity of the models used here. It is possible that more complex domain geometries, boundary conditions, or heterogeneous flows, may change the relationship between K and P , in which case it is unclear if ignoring or switching one of these energy types risks losing accuracy. Exploration of these details is beyond the scope of this paper.

The primary difficulty of using κ_G in a downgradient eddy closure is the presence of the total eddy energy, E , which requires either its own parameterization or prognostic equation. Eden and Greatbatch (2008) overcame a similar challenge with their eddy closure by presenting a prognostic equation for K . As a first step toward incorporating the Marshall et al. (2012) scaling into the GM parameterization, a prognostic equation for E is introduced in the recent work of Mak et al. (2016), so that the completed closure consists of the equation for E and GM parameterization using κ_G , requiring only specification of constant values for both α and the linear eddy energy dissipation rate.

Further work is needed to determine appropriate dissipation operators to use in prognosing the eddy energy, and in particular to develop a skillful parameterization for α . In these simulations it was clear that α varies significantly in time, though the Marshall et al. (2012) scaling demonstrated skill even using a constant value for α . There also appeared to be a tendency for α to asymptote to a near-constant value of 0.2 after the eddy energy saturates, though this may be an artifact of the specific flow geometry considered here. Further investigation is needed using more complex flow scenarios before a more sophisticated parameterization for α can be proposed.

5. Acknowledgements

SB gratefully acknowledges support from the Natural Environment Research Council, award NE/J010472/1. This work was funded by the U.K. Natural Environment Research Council (NE/L005166/1). This work used the ARCHER UK National Supercomputing Service (<http://www.archer.ac.uk>). We would like to thank Stephen Griffies and two anonymous reviewers for comments and insight which greatly improved this manuscript.

Abernathy, R., Ferreira, D. and Klocker, A., 2013. Diagnostics of isopycnal mixing in a circumpolar channel. *Ocean Modelling*, 72, pp. 1-16.

Aiki, H., Jacobson, T. and Yamagata, T., 2004. Parameterizing ocean eddy transports from surface to bottom. *Geophysical Research Letters*, 31, L19302.

Andrews, D.G., 1983. A finite-amplitude Eliassen–Palm theorem in isentropic coordinates. *Journal of the Atmospheric Sciences*, 40(8), pp. 1877-1883.

Andrews, D.G., Holton, J.R. and Leovy, C.B., 1987. *Middle atmosphere dynamics* (No. 40). Academic press.

Andrews, D.G. and McIntyre, M.E., 1976. Planetary waves in horizontal and vertical shear: The generalized Eliassen–Palm relation and the mean zonal acceleration. *Journal of the Atmospheric Sciences*, 33(11), pp. 2031-2048.

473 Aris, R., 2012. Vectors, tensors and the basic equations of fluid mechanics. Courier Corporation.

474 Bachman, S.D. and Fox-Kemper, B., 2013. Eddy parameterization challenge suite I: Eady spindown. *Ocean*
475 *Modelling*, 64, pp. 12-28.

476 Bachman, S.D., Fox-Kemper, B. and Bryan, F.O., 2015. A tracer-based inversion method for diagnosing
477 eddy-induced diffusivity and advection. *Ocean Modelling*, 86, pp. 1-14.

478 Bachman, S.D., Fox-Kemper, B. and Pearson, B. A scale-aware subgrid model for quasigeostrophic turbu-
479 lence. 2016. Submitted to *Journal of Geophysical Research*.

480 Bachman, S.D. and Taylor, J.R., 2016. Numerical simulations of the equilibrium between eddy-induced
481 restratification and vertical mixing. *Journal of Physical Oceanography*, 46(3), pp. 919-935.

482 Bryan, K., Dukowicz, J.K. and Smith, R.D., 1999. On the mixing coefficient in the parameterization of bolus
483 velocity. *Journal of Physical Oceanography*, 29(9), pp. 2442-2456.

484 Cessi, P., 2008. An energy-constrained parameterization of eddy buoyancy flux. *Journal of Physical*
485 *Oceanography*, 38(8), pp. 1807-1819.

486 Chelton, D.B., Deszoeke, R.A., Schlax, M.G., El Naggar, K. and Siwertz, N., 1998. Geographical variability
487 of the first baroclinic Rossby radius of deformation. *Journal of Physical Oceanography*, 28(3), pp. 433-
488 460.

489 Cronin, M., 1996. Eddy-mean flow interaction in the Gulf Stream at 68 W. Part II: Eddy forcing on the
490 time-mean flow. *Journal of Physical Oceanography*, 26(10), pp. 2132-2151.

491 Danabasoglu, G. and Marshall, J., 2007. Effects of vertical variations of thickness diffusivity in an ocean
492 general circulation model. *Ocean Modelling*, 18(2), pp. 122-141.

493 Danabasoglu, G., McWilliams, J.C. and Gent, P.R., 1994. The role of mesoscale tracer transports in the
494 global ocean circulation. *Science*, 264, pp. 1123-1126.

495 Danabasoglu, G. and McWilliams, J.C., 1995. Sensitivity of the global ocean circulation to parameterizations
496 of mesoscale tracer transports. *Journal of Climate*, 8(12), pp. 2967-2987.

497 de Szoeke, R. A., and Bennett, A.F., 1993. Microstructure fluxes across density surfaces. *Journal of Physical*
498 *Oceanography*, 23, pp. 2254-2264.

499 Dukowicz, J.K. and Smith, R.D., 1997. Stochastic theory of compressible turbulent fluid transport. *Physics*
500 *of Fluids* (1994-present), 9(11), pp. 3523-3529.

501 Eady, E.T., 1949. Long waves and cyclone waves. *Tellus*, 1(3), pp. 33-52.

502 Eldén, L., 1982. A weighted pseudoinverse, generalized singular values, and constrained least squares prob-
503 lems. *BIT Numerical Mathematics*, 22(4), pp. 487-502.

504 Eden, C., 2010. Anisotropic rotational and isotropic residual isopycnal mesoscale eddy fluxes. *Journal of*
505 *Physical Oceanography*, 40(11), pp. 2511-2524.

506 Eden, C., 2011. A closure for meso-scale eddy fluxes based on linear instability theory. *Ocean Modelling*,
507 39(3), pp. 362-369.

508 Eden, C. and Greatbatch, R.J., 2008. Towards a mesoscale eddy closure. *Ocean Modelling*, 20(3), pp. 223-
509 239.

510 Eden, C., Jochum, M. and Danabasoglu, G., 2009. Effects of different closures for thickness diffusivity.
511 *Ocean Modelling*, 26(1), pp. 47-59.

512 Farneti, R. and Gent, P.R., 2011. The effects of the eddy-induced advection coefficient in a coarse-resolution
513 coupled climate model. *Ocean Modelling*, 39(1), pp. 135-145.

514 Ferrari, R., Griffies, S.M., Nurser, A.G. and Vallis, G.K., 2010. A boundary-value problem for the parame-
515 terized mesoscale eddy transport. *Ocean Modelling*, 32(3), pp. 143-156.

516 Ferrari, R., McWilliams, J.C., Canuto, V.M. and Dubovikov, M., 2008. Parameterization of eddy fluxes near
517 oceanic boundaries. *Journal of Climate*, 21(12), pp. 2770-2789.

518 Ferreira, D. and Marshall, J., 2006. Formulation and implementation of a residual-mean ocean circulation
519 model. *Ocean Modelling*, 13(1), pp. 86-107.

520 Ferreira, D., Marshall, J. and Heimbach, P., 2005. Estimating eddy stresses by fitting dynamics to observa-
521 tions using a residual-mean ocean circulation model and its adjoint. *Journal of Physical Oceanography*,
522 35(10), pp. 1891-1910.

523 Fox-Kemper, B., Ferrari, R. and Hallberg, R., 2008. Parameterization of mixed layer eddies. Part I: Theory
524 and diagnosis. *Journal of Physical Oceanography*, 38(6), pp. 1145-1165.

525 Fox-Kemper, B., Lumpkin, R. and Bryan, F.O., 2013. Lateral transport in the ocean interior. *Ocean Circula-
526 tion and Climate: A 21st century perspective*, 103, pp. 185-209.

527 Fox-Kemper, B., and Menemenlis, D., 2008. Can large eddy simulation techniques improve mesoscale rich
528 ocean models? *Geophysical Monograph Series*, 177, pp. 319-337.

529 Gaspar, P., Grégoris, Y. and Lefevre, J.-M., 1990. A simple eddy kinetic energy model for simulations of
530 the oceanic vertical mixing: Tests at station Papa and Long-Term Upper Ocean Study site. *Journal of
531 Geophysical Research: Oceans*, 95(C9), pp. 16179-16193.

532 Gent, P.R., 2011. The GentMcWilliams parameterization: 20/20 hindsight. *Ocean Modelling*, 39(1), pp. 2-9.

533 Gent, P.R., and McWilliams, J.C., 1990. Isopycnal mixing in ocean circulation models. *Journal of Physical
534 Oceanography*, 20(1), pp. 150-155.

535 Gent, P.R., Willebrand, J., McDougall, T.J. and McWilliams, J.C., 1995. Parameterizing eddy-induced tracer
536 transports in ocean circulation models. *Journal of Physical Oceanography*, 25(4), pp. 463-474.

537 Greatbatch, R.J., 1998. Exploring the relationship between eddy-induced transport velocity, vertical momen-
538 tum transfer, and the isopycnal flux of potential vorticity. *Journal of Physical Oceanography*, 28(3), pp.
539 422-432.

540 Green, J.S.A., 1970. Transfer properties of the large-scale eddies and the general circulation of the atmo-
541 sphere. *Quarterly Journal of the Royal Meteorological Society*, 96(408), pp. 157-185.

542 Griffies, S.M., 1998. The Gent–McWilliams skew flux. *Journal of Physical Oceanography*, 28(5), pp. 831-
543 841.

544 Griffies, S.M., 2004. Fundamentals of ocean climate models (Vol. 518, No. 1). Princeton: Princeton Univer-
545 sity Press.

546 Griffies, S.M., Gnanadesikan, A., Pacanowski, R.C., Larichev, V.D., Dukowicz, J.K. and Smith, R.D., 1998.
547 Isoneutral diffusion in a z -coordinate ocean model. *Journal of Physical Oceanography*, 28(5), pp. 805-830.

548 Hallberg, R., 2013. Using a resolution function to regulate parameterizations of oceanic mesoscale eddy
549 effects. *Ocean Modelling*, 72, pp. 92-103.

550 Harcourt, R.R., 2015. An improved second-moment closure model of Langmuir turbulence. *Journal of Phys-
551 ical Oceanography*, 45, pp. 84-103. doi: <http://dx.doi.org/10.1175/JPO-D-14-0046.1>

552 Hecht, M. W. and Smith, R.D., 2008. Toward a physical understanding of the North Atlantic: A review of
553 model studies in an eddying regime. *Ocean Modeling in an Eddying Regime*, AGU Geophysical Mono-
554 graph 177, pp. 213-240.

555 Henning, C. C. and Vallis, G.K., 2004. The effects of mesoscale eddies on the main subtropical thermocline.
556 *Journal of Physical Oceanography*, 34(11), pp. 2428-2443.

557 Hoskins, B.J., James, I.N. and White, G.H., 1983. The shape, propagation and mean-flow interaction of
558 large-scale weather systems. *Journal of the Atmospheric Sciences*, 40(7), pp. 1595-1612.

559 Jansen, M.F., Adcroft, A.J., Hallberg, R. and Held, I.M., 2015. Parameterization of eddy fluxes based on a
560 mesoscale energy budget. *Ocean Modelling*, 92, pp.28-41.

561 Jones, D.C., Ito, T., Birner, T., Klocker, A. and Munday, D., 2015. Planetary-geometric constraints on
562 isopycnal slope in the Southern Ocean. *Journal of Physical Oceanography*, 45(12), pp. 2991-3004.

563 Killworth, P.D., 1997. On the parameterization of eddy transfer Part I. Theory. *Journal of Marine Research*,
564 55(6), pp. 1171-1197.

565 Lauderdale, J.M., Naveira Garabato, A.C., Oliver, K.I., Follows, M.J. and Williams, R.G., 2013. Wind-
566 driven changes in Southern Ocean residual circulation, ocean carbon reservoirs and atmospheric CO₂.
567 *Climate Dynamics*, 41(7-8), pp. 2145-2164.

568 Lee, M.M., Marshall, D.P. and Williams, R.G., 1997. On the eddy transfer of tracers: Advective or diffusive?
569 *Journal of Marine Research*, 55(3), pp. 483-505.

570 Maddison, J.R. and Marshall, D.P., 2013. The Eliassen-Palm flux tensor. *Journal of Fluid Mechanics*, 729,
571 pp. 69-102.

572 Mak, J., Marshall, D.P., Maddison, J.R. and Bachman, S.D., 2016. Emergent eddy saturation from an energy
573 constrained eddy parameterization. Submitted to *Ocean Modelling*.

574 Marshall, D.P. and Adcroft, A.J., 2010. Parameterization of ocean eddies: Potential vorticity mixing, ener-
575 getics and Arnold's first stability theorem. *Ocean Modelling*, 32(3), pp. 188-204.

576 Marshall, D.P., Maddison, J.R. and Berloff, P.S., 2012. A framework for parameterizing eddy potential
577 vorticity fluxes. *Journal of Physical Oceanography*, 42(4), pp. 539-557.

578 Marshall, J., Adcroft, A., Hill, C., Perelman, L. and Heisey, C., 1997. A finite-volume, incompressible
579 Navier Stokes model for studies of the ocean on parallel computers. *Journal of Geophysical Research: Oceans*, 102(C3), pp. 5753-5766.

581 Marshall, J. and Speer, K., 2012. Closure of the meridional overturning circulation through Southern Ocean
582 upwelling. *Nature Geoscience*, 5(3), pp. 171-180.

583 Mazloff, M.R., Heimbach, P. and Wunsch, C., 2010. An eddy-permitting Southern Ocean state estimate.
584 *Journal of Physical Oceanography*, 40(5), pp. 880-899.

585 McDougall, T.J., 1987. Neutral surfaces. *Journal of Physical Oceanography*, 17(11), pp. 1950-1964.

586 McDougall, T.J. and McIntosh, P.C., 2001. The temporal-residual-mean velocity. Part II: Isopycnal interpre-
587 tation and the tracer and momentum equations. *Journal of Physical Oceanography*, 31(5), pp.1222-1246.

588 McIntosh, P.C. and McDougall, T.J., 1996. Isopycnal averaging and the residual mean circulation. *Journal*
589 *of Physical Oceanography*, 26(8), pp. 1655-1660.

590 Mellor, G.L. and Yamada, T., 1982. Development of a turbulence closure model for geophysical fluid prob-
591 lems. *Reviews of Geophysics*, 20(4), pp. 851-875.

592 Middleton, J.F. and Loder, J.W., 1989. Skew fluxes in polarized wave fields. *Journal of Physical Oceanogra-*
593 *phy*, 19(1), pp. 68-76.

594 Müller, P. and Garrett, C., 2002. From stirring to mixing in a stratified ocean. *Oceanography* 15, 12-19.

595 Munday, D.R., Johnson, H.L. and Marshall, D.P., 2013. Eddy saturation of equilibrated circumpolar currents.
596 *Journal of Physical Oceanography*, 43(3), pp. 507-532.

597 Nycander, J., 2011. Energy conversion, mixing energy, and neutral surfaces with a nonlinear equation of
598 state. *Journal of Physical Oceanography*, 41(1), pp. 28-41.

599 Pearson, B., Fox-Kemper, B. and Bachman, S.D. Subgrid schemes affect global mesoscale ocean large eddy
600 simulations. 2016. Submitted to *Journal of Geophysical Research*.

601 Pedlosky, J., 2013. *Geophysical Fluid Dynamics*. Springer Science and Business Media.

602 Plumb, R.A., 1979. Eddy fluxes of conserved quantities by small-amplitude waves. *Journal of the Atmo-*
603 *spheric Sciences*, 36(9), pp. 1699-1704.

604 Plumb, R.A., 1986. Three-dimensional propagation of transient quasigeostrophic eddies and its relationship
605 with the eddy forcing of the time-mean flow. *Journal of the Atmospheric Sciences*, 43(16), pp.1657-1678.

606 Plumb, R.A. and Mahlman, J.D., 1987. The zonally averaged transport characteristics of the GFDL general
607 circulation/transport model. *Journal of the Atmospheric Sciences*, 44(2), pp. 298-327.

608 Prandtl, L., 1925. Bericht ber Untersuchungen zur ausgebildeten Turbulenz. *Z. Angew. Math. Mech*, 5(2),
609 pp. 136-139.

610 Redi, M.H., 1982. Oceanic isopycnal mixing by coordinate rotation. *Journal of Physical Oceanography*,
611 12(10), pp. 1154-1158.

612 Rodi, W., 1993. *Turbulence models and their application in hydraulics*. CRC Press.

613 Smith, K.S. and Marshall, J., 2009. Evidence for enhanced eddy mixing at middepth in the Southern Ocean.
614 *Journal of Physical Oceanography*, 39(1), pp. 50-69.

- 615 Smith, R.D. and Gent, P.R., 2004. Anisotropic Gent–McWilliams parameterization for ocean models. *Journal of Physical Oceanography*, 34(11), pp. 2541-2564.
- 616
- 617 Stammer, D., 1997. Global characteristics of ocean variability estimated from regional TOPEX/POSEIDON altimeter measurements. *Journal of Physical Oceanography*, 27(8), pp. 1743-1769.
- 618
- 619 Stone, P.H., 1972. A simplified radiative-dynamical model for the static stability of rotating atmospheres. *Journal of the Atmospheric Sciences*, 29(3), pp. 405-418.
- 620
- 621 Taylor, G.I., 1921. Diffusion by continuous movements. *Proc. London Math. Soc.*, 20(1), pp. 196-212.
- 622 Treguier, A.M., Held, I.M. and Larichev, V.D., 1997. Parameterization of quasigeostrophic eddies in primitive equation ocean models. *Journal of Physical Oceanography*, 27(4), pp. 567-580.
- 623
- 624 Vallis, G.K., 2006. *Atmospheric and Oceanic Fluid Dynamics: Fundamentals and Large-Scale Circulation*. Cambridge University Press.
- 625
- 626 Visbeck, M., Marshall, J., Haine, T. and Spall, M., 1997. Specification of eddy transfer coefficients in coarse-resolution ocean circulation models. *Journal of Physical Oceanography*, 27(3), pp. 381-402.
- 627
- 628 Wardle, R. and Marshall, J., 2000. Representation of eddies in primitive equation models by a PV flux. *Journal of Physical Oceanography*, 30(10), pp. 2481-2503.
- 629
- 630 Young, W.R., 2010. Dynamic enthalpy, conservative temperature, and the seawater Boussinesq approximation. *Journal of Physical Oceanography*, 40(2), pp. 394-400.
- 631
- 632 Young, W.R., 2012. An exact thickness-weighted average formulation of the Boussinesq equations. *Journal of Physical Oceanography*, 42(5), pp. 692-707.
- 633
- 634 Zhao, R. and Vallis, G., 2008. Parameterizing mesoscale eddies with residual and Eulerian schemes, and a comparison with eddy-permitting models. *Ocean Modelling*, 23(1), pp. 1-12.
- 635

636 **Appendix A. Gent and McWilliams in the QG approximation**

637 The diagnostics discussed in this article are performed via zonal averaging at constant height, and in particular the GM coefficient is derived via an eddy buoyancy flux defined in terms of averages and perturbations at constant height. However the GM scheme is more precisely a closure for the difference between the velocity averaged at constant height, and the velocity thickness-weighted averaged at constant buoyancy (see in particular McDougall and McIntosh, 2001, section 10.a.). Here the differences between constant height and constant buoyancy averaging are outlined, and the eddy transport velocity in the QG limit, derived in Treguier et al. (1997), is discussed.

644 Consider the buoyancy equation in the form

$$\frac{\partial b}{\partial t} + \nabla_3 \cdot (\mathbf{u}b) = 0 \quad (\text{A.1})$$

645 where the velocity \mathbf{u} is assumed non-divergent. Introduce an average at constant height operator $\overline{(\dots)}^z$ with associated eddy operator $(\dots)^{\prime z}$. The constant height averaged buoyancy equation is then

$$\frac{\partial \bar{b}}{\partial t} + \nabla_3 \cdot (\bar{\mathbf{u}}^z \bar{b}^z) = -\nabla_3 \cdot (\bar{\mathbf{u}}^{\prime z} \bar{b}^{\prime z}). \quad (\text{A.2})$$

647 where $\bar{\mathbf{u}}^z$ is non-divergent.

648 Now introduce an average at constant buoyancy operator $\overline{(\dots)}|_{b^\#}$. This operator is described in Mc-
 649 Dougall and McIntosh (2001), where it is defined in terms of the density. A thickness-weighted average of
 650 a scalar field ϕ is defined (e.g. Andrews, 1983; Young, 2012)

$$\hat{\phi} = \overline{\phi \left(\frac{\partial b}{\partial z} \right)^{-1}} \bigg|_{b^\#} \frac{\partial b^\#}{\partial z} \quad (\text{A.3})$$

651 where $b^\# = \overline{b}|_{b^\#}$ is the buoyancy averaged at constant buoyancy (and is the quantity $b^\#$ in Young, 2012). The
 652 thickness-weighted averaged buoyancy equation is then (McDougall and McIntosh, 2001, equation (26))

$$\frac{\partial b^\#}{\partial t} + \nabla_3 \cdot (\hat{\mathbf{u}} b^\#) = 0, \quad (\text{A.4})$$

653 where $\hat{\mathbf{u}} = (0, \hat{v}, \omega)$ and where ω is defined so that $\hat{\mathbf{u}}$ is non-divergent. The eddy transport velocity is defined
 654 (McDougall and McIntosh, 2001)

$$\mathbf{u}^* = \hat{\mathbf{u}} - \bar{\mathbf{u}}^z. \quad (\text{A.5})$$

655 Subtracting equation (A.2) from equation (A.4) leads to

$$\nabla_3 \cdot (\overline{\mathbf{u}^z b'^z}) = \nabla_3 \cdot (\mathbf{u}^* b^\#) + \partial_t b^* + \nabla_3 \cdot (\bar{\mathbf{u}}^z b^*), \quad (\text{A.6})$$

656 where

$$b^* = b^\# - \bar{b}^z. \quad (\text{A.7})$$

657 The GM parameterization defines the eddy induced advection \mathbf{u}^* of thickness-weight averaged tracers
 658 (McDougall and McIntosh, 2001). Up to differences arising from a non-linear equation of state, this yields a
 659 closure for the first right-hand-side term in equation (A.6). This differs from the eddy buoyancy flux diver-
 660 gence defined via constant height averaging by terms involving the difference between the mean buoyancies,
 661 b^* .

662 Under quasigeostrophic scaling, assuming that relevant eddy and mean quantities are of the same order
 663 in Rossby number, to leading order in Rossby number equation (A.6) leads to an ageostrophic transport
 664 velocity as per Treguier et al. (1997), with

$$\nabla_h \cdot (\overline{\mathbf{u}_g^z b'^z}) = w_{ag}^* \mathcal{N}_0^2, \quad (\text{A.8})$$

665 where \mathbf{u}_g is the geostrophic velocity and $\mathcal{N}_0^2 = db_0/dz \approx \partial \bar{b}^z / \partial z$. This is the definition applied in the
 666 derivation of the residual-mean QG equations (see e.g. the appendix of Marshall et al., 2012).